Proceedings of the 20th International Conference on Soil Mechanics and Geotechnical Engineering– Rahman and Jaksa (Eds)

A new fabric evolution monitoring method using continuous bidirectional shear wave velocity measurements in sand

Une nouvelle méthode de surveillance de l'évolution de la structure du sol utilisant des mesures continues de la vitesse des ondes de cisaillement bidirectionnelles dans le sable

Kazem Fakharian
Department of Civil and Environmental Engineering, Amirkabir University of Technology, Iran, kfakhari@aut.ac.ir

Frazad Kaviani-Hamedani
Amirkabir University of Technology, Iran

Ali Sooraki & Mostafa Amindehghan
Student at Amirkabir University of Technology, Iran

ABSTRACT: Sensible fabric evolution monitoring of crushed, sandy specimens during shearing up to critical state is enabled by the addition of continuous, bidirectional shear wave velocity measurements along the vertical and horizontal directions (V&H). Two specially designed horizontal bender element housing are mounted on triaxial samples using a new technique easing installation and sealing the H-housing. The specimens are prepared by water sedimentation methods and then subjected to strain-controlled, compression and extension loading under drained conditions. Not only do the differences between shear wave velocities in different directions illuminate a severe and increasing soil anisotropy during the shearing, but also the results correspond to significant information related to the current fabric and stress state as well. Comparison between compression and extension results highlight different fabric evolution trends and consequently dissimilar fabric states at the critical as well. The Variations of the utilized fabric function underline the fact that there is a unique but anisotropic fabric at the critical state. Considering the meaningful results compared to recent findings derived from discrete element method (DEM), the proposed method can be used as an experimental method facilitating the macroscopic evaluation of fabric anisotropy in granular materials.

Résumé: La surveillance de l'évolution sensible de la structure d'échantillons sableux broyés pendant le cisaillement jusqu'à l'état critique est rendue possible par l'ajout de mesures continues et bidirectionnelles de la vitesse des ondes de cisaillement le long des directions verticale et horizontale (V&H). Deux boîtiers d'éléments piézocéramique horizontaux spécialement conçus sont montés sur des échantillons triaxiaux en utilisant une nouvelle technique facilitant l'installation et l'étanchéité du boîtier-H. Les échantillons sont préparés par des méthodes de sédimentation dans l'eau, puis soumis à des charges de compression et extension contrées par la déformation dans des conditions drainées. Non seulement les différences entre les vitesses des ondes de cisaillement dans différentes directions mettent en évidence une anisotropie sévère et croissante du sol pendant le cisaillement, mais les résultats correspondent également à des informations significatives liées à la structure actuelle et à l'état de contrainte. La comparaison entre les résultats de compression et d'extension mettent en évidence différentes tendances d'évolution de la structure et, par conséquent, des états différents de la structure à l'état critique. Les variations de la fonction de structure utilisée soulignent le fait qu'il existe une structure unique mais anisotrope à l'état critique. Compte tenu des résultats significatifs par rapport aux découvertes récentes dérivées de la méthode des éléments discrets (MED), la méthode proposée peut être utilisée comme une méthode expérimentale facilitant l'évaluation macroscopique de l'anisotropie de la structure dans les matériaux granulaires.

KEYWORDS: Fabric evolution, bender element test, shear wave velocity, critical state, image processing

1 INTRODUCTION

Monotonic and cyclic responses of granular materials are greatly affected by different crucial factors such as relative density, confining pressure, and microscopic characteristics. Sandy soils, as a granular material, behave anisotropically due to the intrinsic microscopic characteristics called soil fabric. Apart from a few experimental studies on the effect of sample preparation methods which provide different initial soil fabric (Miura et al., 1982; Tatsuoka et al., 1986; Guo, 2008; Yu et al., 2013), the importance of soil fabric and its evolution during shearing mostly have been investigated using discrete element method (DEM) and tomography inspections. These methods, however, are time-consuming and expensive, considering their undeniable values (Zhao and Guo, 2013; Zhao et al., 2013; Cheng and Wang, 2018). To consider the interrelated parameters convoluting the prediction of soil responses, the recent constitutive models employing different frameworks are attemptting to involve the soil anisotropy and the role of the soil fabric.

Classical critical state theory was developed by Roscoe et al. (1958) and Schofield et al. (1968), predicting the soil response in which the soil specimens at critical state implicitly have an isotropic fabric state. However, soils tend to behave anisotropically during shearing, and there are strong shreds of evidence that fabric becomes greatly anisotropic at critical state (Nakakuki and Oda, 1972; Masson and Martinez, 2001; Li and Li, 2009). Moreover, recent DEM simulations indicated that the soil fabric not only exhibits an anisotropic state at the critical state, but also experiences a severe fabric evolution from the initial state towards a unique critical state. Such observations has been disregarded in the classical critical state (Li and Dafalias, 2012; Yan and Zhang, 2013).

On the other hand, soil stiffness at very small strain (G_0) can greatly be influenced by microscopic characteristics such as grain arrangements, grain roughness, and grain contacts. Shear wave velocities (i.e., V_{vh}, V_{hv}, and V_{hh}) and corresponding shear moduli (i.e., G_{vh}, G_{hv}, and G_{hh}) have been measured and monitored using a common laboratory test called bender element test that involves transmitting and receiving shear waves using

small electro-mechanical transducers (Shirley and Hampton, 1978). Continuous monitoring of bender element measurements during triaxial testing were performed along vertical direction by Styler and Howie (2014). Besides, similar consecutive shear wave velocity measurements during axial compression shearing were conducted up to the critical state by Fakharian et al. (2019), Kaviani-Hamedani et al. (2021), and Fakharian et al. (2021). The results showed that despite the differences in initial values of shear wave velocities before subjecting the specimen to shear loading, they experienced considerable changes due to variations in stress states and density and reached a critical value after a fairly large amount of axial strain. Therefore, the values of shear wave velocities approach a unique critical value irrespective of the initial stiffness values. Moreover, the findings of authors' previous studies demonstrated that the initial stiffness anisotropy becomes more pronounced at the critical state compared with the initial state. Therefore, continuous monitoring of shear wave velocities, particularly the bidirectional monitoring, provide meaningful results which had been previously observed only in DEM simulations and can play the role of useful experimental evidences corresponding to the microscopic investigations.

The main objective of this paper is conducting bidirectional shear wave velocity measurements during drained axial compression and extension shearing on a crushed silica sand up to the critical state, highlighting fabric evolution. The experiments are carried out using an automated triaxial apparatus accompanied by four bender elements for continuous measurements of the V_{vh} and V_{hh} variations.

2 TESTING APPARATUS AND MEASURING DEVICES

2.1 *Triaxial apparatus and image processing*

In this study, an automated triaxial apparatus capable of closed-loop control was used to perform the experiments. Measurements of V_{vh} and V_{hh} required current tip-to-tip travel distances between transmitter and receiver bender ceramics in both directions at any loading state, which were measured using different methods. The current vertical traveling distance was obtained by subtraction of the axial deformation (measured by an LVDT) from the initial height of the specimen. However, accurate horizontal traveling distance measurements were carried out employing an image processing method. A rigid frame was mounted onto the device frame to place a camera in front of the triaxial cell (Figure 1). The radial deformations of the specimen, and subsequently variations of travel distance in the H-direction, were accurately measured at different loading times. The image processing was conducted using two image processing software (Ncorr-Open source 2D digital image correlation MATLAB and ImageJ) to identify the failure pattern and horizontal traveling distance (Harilal et al., 2014). For more details in the verification of image processing, please refer to Fakharian et al. (2019) and Kaviani-Hamedani et al. (2021).

2.2 Horizontal bender element mounting

The placement of on-sample horizontal bender elements is a difficult and delicate task considering the sealing challenge. The proposed methodology used in this study is presented in Figure 2(a). The assembly includes latex earrings, bender capsules, bender housings, three rotary sealing, and several O-rings. Latex earring provides a sealant coating for the inner assembly of horizontal bender elements, and the bender housing is installed into the double-acting rotary sealing, which seals statically against any leakage from the cell chamber to the specimen and vice versa. Several O-rings seal the contact of latex earrings and bender element capsules effectively.

In Figure 2(b), a cross-sectional view of equipment during specimen preparation is presented. This assembly facilitates specimen preparation using different methods including wet tamping and water sedimentation methods. The horizontal bender capsules are placed within the outer earings which are also sealed using a pair of outer packers.

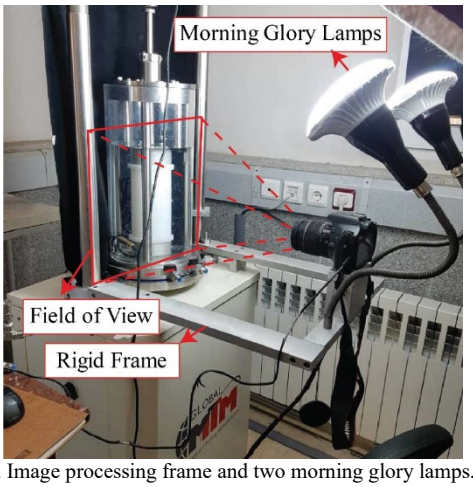

Figure 1. Image processing frame and two morning glory lamps.

3 TESTING MATERIAL AND SPECIMEN PREPARATION

3.1 *Material properties*

The soil used in this study is a crushed silica sand known as Firuzkuh F161. It is a gap graded, subangular sand and manufactured industrially with crusher nearby Tehran, Iran. Gradation curve of Firuzkuh sand according to ASTM D 422 (2007) standard is presented in Figure 3(a). In Figure 3(b) the results of volume rendering of micro CT scan images of Firuzkuh sand is presented to have a better understanding of particle shapes. The the grains are subangular to subrounded with average sphericity of 0.69. Physical properties of the Firuzkuh sand are outlined in Table 1. The stress-strain response for Firuzkuh sand has also been characterized under different stress paths using undrained triaxial and hollow cylinder apparatuses (e.g., Eghbali and Fakharian, 2014; Fakharian et al., 2018; Ahmad and Fakharian, 2020; Fakharian and Vafaie, 2021; Vafaei et al. 2021).

3.2 Specimen preparation

A set of experiments containing eleven drained axial compression and extension triaxial experiments (i.e., six compression and 5 extension tests) were conducted. The diameter and height of samples are 71 mm and 160 mm, respectively. The samples were prepared by Water Sedimentation (WS) method. The H bender element ceramics are inserted into the bender capsule before sedimentation procedure, while vertical bender element probes are pre-mounted in the upper plate and the pedestal for vertical wave propagations.

The WS specimens were produced using the procedure proposed by Chern (1981). Strain-controlled shearing of specimens are performed after the isotopic consolidation. Bidirectional measurement of shear wave velocities in vertical and horizontal directions is scheduled to commence as shearing starts.

4 TEST PROGRAM

Details of the test program is outlined in Table 2. The void ratio and relative density at the end of consolidation are presented in the table. The void ratio at the end of the test was achieved by the proposed method of Verdugo and Ishihara (1996). The

specimens were isotropically consolidated with $p' = (\sigma'_v + 2\sigma'_h)/3 = 100$ or 200 kPa and $q = \sigma'_v - \sigma'_h = 0$.

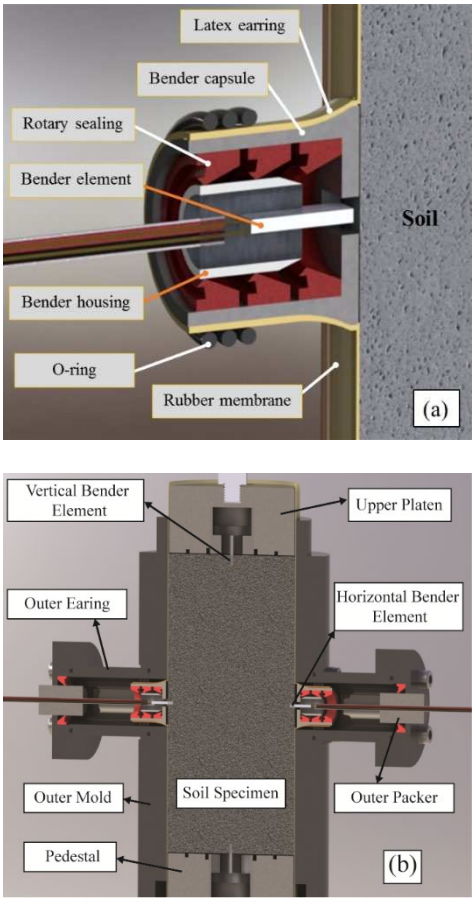

Figure 2. Proposed installation method of horizontal bender elements: (a) H bender element installation; (b) cross-sectional view of the outer mold.

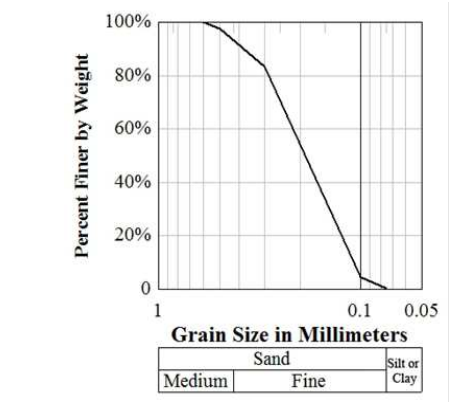

(a)

(b)

Figure 3. Morphology of Firuzkuh sand F-161: (a) Gradation; (b) The volume rendering of Micro CT images.

Table 1. Physical properties of Firuzkuh sand F-161.

C_c	C_u	D_{50} (mm)	G_s	e_{max}	e_{min}
0.88	1.9	0.22	2.65	0.931	0.56

5 SIGNAL INTERPRETATION

Signal interpretation with the aim of travel time determination is a challenging task onto which there has been a significant amount of research (e.g., Lee and Santamarina 2005; Da Fonseca et al. 2009). Travel time of both Vvh and Vhh were measured during shearing using the peak to peak method. Figure 4 presents an example of travel time measurement during the entire shearing path performed on specimen DR25-P100 in the horizontal direction. As shown in Figure 4, the received waves have lied deliberately onto each other for a better understanding of changes in the received signals in such a way that the first and the last received signals pertain to the end of consolidation (EOC) and the Critical State (CS) stages, respectively.

Table 2. Outline of the test program.

Test name	p'_c (kPa)	e	D_r (%)	Loading mode
DR24-P100	100	0.841	24	Compression
DR25-P100	100	0.838	25	Compression
DR26-P100	100	0.834	26	Compression
DR29-P200	200	0.823	29	Compression
DR31-P200	200	0.815	31	Compression
DR32-P200	200	0.812	32	Compression
E-DR17-P100	100	0.845	23	Extension
E-DR18-P100	100	0.841	24	Extension
E-DR27-P100	200	0.808	33	Extension
E-DR28-P100	200	0.804	34	Extension
E-DR29-P100	200	0.800	35	Extension

The other waves are captured during the specimen shearing and represent the shear wave velocities in different loading stages (various deformation).

Aside from some translocations in the x-direction, the waveform of the received signals at various stages remained constant. The translocations in the received signals led to a stepwise variation in shear wave velocity. The peak-to-peak signal interpretation treats the elapsed time between the first peak of transmitted signal and the first major peak of the received signal as the travel time. The locus of the first major peak of received signals is illustrated by a black line passing through the mentioned peak points (Figure 4).

The horizontal and vertical travel distances were measured in an undisturbed manner using an image processing method and an axial LVDT, respectively. Figure 5(a) presents the image processing results for one specimen onto which the horizontal and the vertical displacement contours are overlaid. The general pattern of failure for compression and extension specimens are bulging and necking, and as expected, the horizontal bender elements recede and approach each other, respectively (Figure 5(b)).

6 TEST RESULTS

Figure 6 shows the stress-strain responses of axial compression and extension experiments under 100 and 200 kPa of p'_c. The maximum axial strain for compression and extension tests are 16% and 10%, respectively. As expected, deviatoric stress curves

exhibit greater values at the end of tests as p'_c changes from 100 to 200 kPa, and have the same values for a specific p'_c by approaching the critical state. Following this, Figure 7 shows the void ratio values of all specimens approaching the corresponding critical state lines of compression and extension loading modes. The plotted critical state line are based on authors' previous studies using undrained triaxial experiments (Lashkari et al., 2017; Fakharian and Kaviani-Hamedani, 2020). The curves of void ratios clearly exhibit the contractive-dilative behavior (i.e., decrease and then increase in the void ratio) by passing through a diverting point known as the phase transformation point and approach a critical void ratio for a given p'_c, irrespective of initial values of the void ratio.

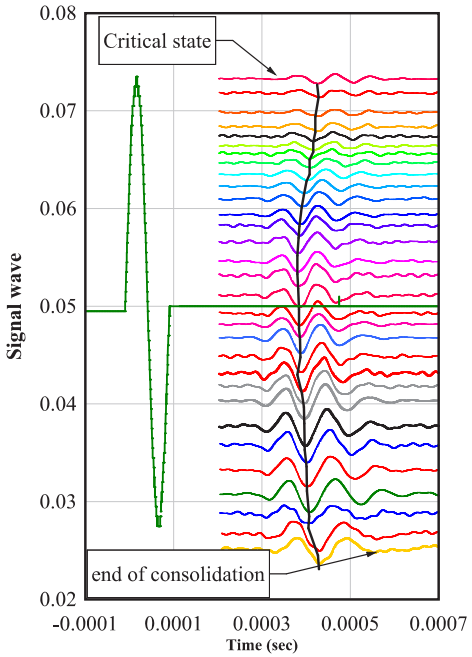

Figure 4. Trend of travel time of horizontal direction of TD25PD100 specimen from EOC to critical state.

Figure 8 presents Vvh and Vhh curves against axial strain for compression and extension loading modes. Figure 8(a) compares the variations of Vvh and Vhh for specimens consolidated under 100 kPa of p'_c. Vvh and Vhh grow from initial values, representing stiffness of specimens at the end of consolidation, and after passing peak points decline towards a critical value. As shown, there is a negligible difference in Vvh and Vhh at the beginning of shearing, representing initial stiffness anisotropy, and the curves of Vvh and Vhh strat to recede from each other after the peak points, highlighting an increase in stiffness anisotropy. This increasing pattern is more pronounced for specimens with p'_c=200 kPa, which are plotted in Figure 7(b). Comparing parts (a) and (b) of Figure 7, considering the differences at the critical values of Vvh and Vhh, these values are greatly increased when p'_c changes from 100 kPa to 200 kPa so that the critical values of Vvh and Vhh for 100 and 200 kPa are 180 and 170, and 230 and 190, respectively.

Similar to parts (a) and (b), parts (c) and (d) of Figure 7 compare the changes in V_{vh} and V_{hh} values versus axial strain for extension experiments with p'_c=100 and 200 kPa, respectively. Unlike changing patterns in V_{vh} and V_{hh} of compression experiments for which the V_{vh} curves exceeded V_{hh} curves as shearing commence, a reverse pattern can be observed in extension mode so that the V_{vh} curves instantly drop as the shearing commences and then reach a plateau at a fairly large amount of axial stain or by approaching the critical state. However, V_{hh} curves have exhibited a slight decrease as shearing starts and then experience a gradual growth up to the critical state, and this pattern is more apparent for p'_c=100 kPa. Therefore, compare to presented changes under compression loading, in which shear wave velocity values along the vertical direction clearly exceeded corresponding values along the horizontal direction, there is a reverse changing pattern under extension loading mode, highlighting a significant difference in fabric evolution between compression and extension loading modes.

Recent research has indicated that shear waves propagate within particular materials using micro-mechanisms that are strongly influenced by some microstructural factors. Some recent studies illuminated the dominant role of micromechanical characteristics underlying stress exponents such as normal contact forces, normal contacts, and coordination number – the average contact numbers per particle (Wang and Mok, 2008; Gu and Yang, 2013).

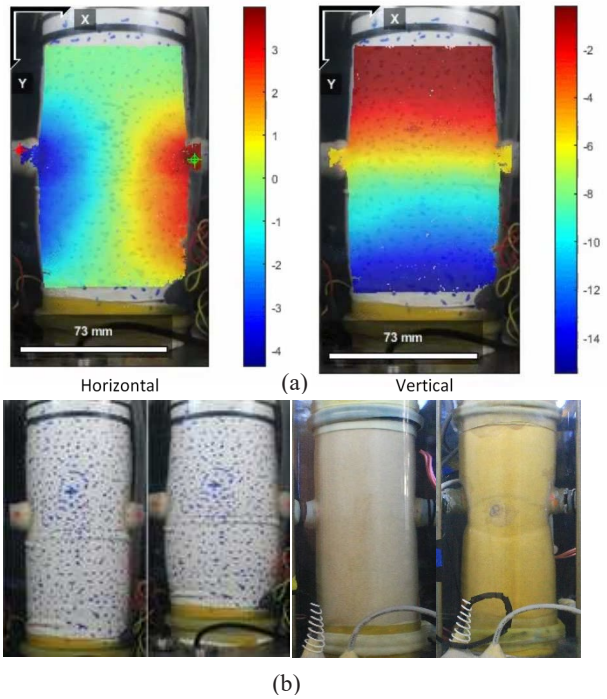

Figure 5. Deformed shape of specimens under shearing: (a) The horizontal and vertical displacement contours in compression mode; (b) Failure modes of specimens at the end of testsl.

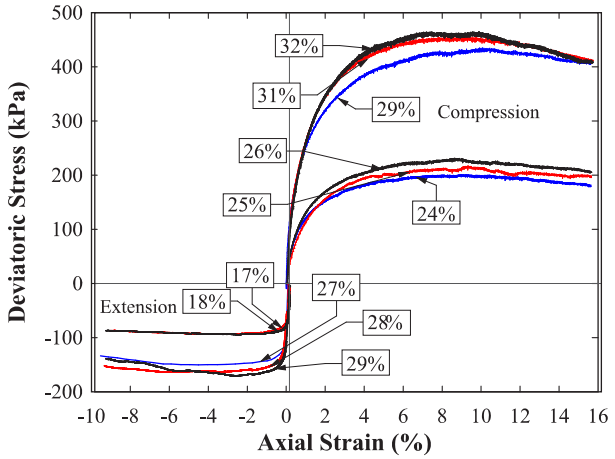

Figure 6. Stress-strain responses of specimens subjected to axial compression and extension loading.

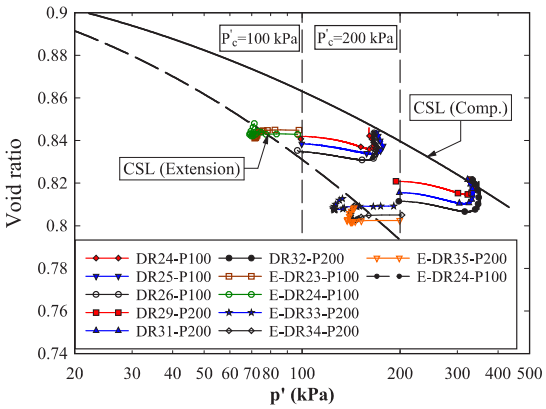

Figure 7. Variations of void ratio up to the critical state lines in $e - \ln p'$ plane.

It seems that the difference in changing pattern underlines the fact that an axial compression loading strengthens and weakens the specimen fabric by the creation and disruption of many contact points in vertical and horizontal directions, respectively, and a reverse pattern of fabric evolution can be expected for extension loading mode. Therefore, this difference in fabric evolution between compression and extension loading can explain the underlying reason for the dissimilarity of shear wave changes between axial compression and extension shearing. The differences in changing patterns lead to different critical stiffness and consequently dissimilar fabric states at critical state as well, which explain the distinction between CSL of compression and extension modes.

Moreover, Figure 7 clearly demonstrates that the negligible initial stiffness anisotropy becomes intense by approaching the critical state, which is in agreement with recent DEM results (Yan and Zhang, 2013; Zhao et al., 2013; Yang et al., 2016). The rate of changes in shear wave velocities also depreciates at large amounts of strain due to the reduction of changes in the stress state and micromechanical characteristics such as coordination number.

In parts (c) and (d) of Figure 7, the curves of V_{hh} scattered when the necking shear band appeared (i.e., 5% of axial strain). It is expected that the possible slight rotation of H bender element housings, adjacent effect of necking on stress state, and changes in location of the shear band are responsible for the observed scattering. Similar scattering at the lower level can also be seen among compression specimens.

7 CONCLUSIONS

The possibility of continuous bidirectional monitoring of sh ear wave velocities during shearing in which two horizonta l piezo-electrics were mounted on samples using a new m easurement technique was examined. This was made feasib le by three rotary seals implanted in bender capsules. A se ries of drained triaxial compression and extension tests wer e performed on the crushed Firuzkuh silica sand. The vari ations of shear wave velocities in different directions were investigated to evaluate soil anisotropy and fabric. Shear w ave velocity measurements using bender element tests were found pregnant with useful information describing fabric e volution, and the variation of shear wave velocities was ex plained using recent micromechanical findings. The main fi ndings of this study are as summarized as follows:

1. All specimens approach a critical shear wave velocity at the end of tests for a given p'_c and loading mode, irrespective of the initial states.
2. It was observed that shearing mode has a significant impact on the changing pattern of shear wave changes during shearing so that there was a totally reversed pattern in compression and extension modes, due to a clear difference in fabric evolution.
3. Despite the negligible initial stiffness anisotropy at th e of consolidation, the stiffness anisotropy becomes si gnificant, underscoring recent findings of DEM simul ations.
4. The soil fabric at large axial strains is supposed to b e unique and anisotropic, greatly influenced by sheari ng mode and irrespective of the initial state.

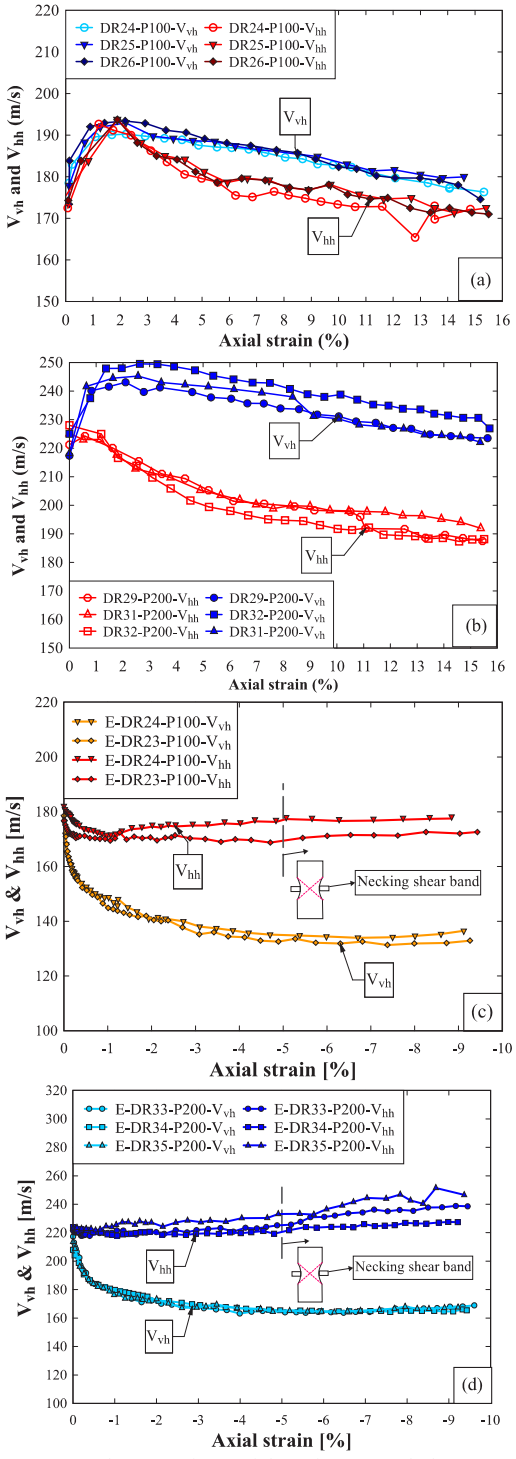

Figure 8. V_{vh} and V_{hh} against axial strain: (a) and (b) compression shearing with $p'_c = 100$ kPa and 200 kPa, respectively; (c) and (d) extension shearing with $p'_c = 100$ kPa and 200 kPa, respectively.

8 ACKNOWLEDGEMENTS

The authors would like to acknowledge the contributions of Global Material Testing Manufacturers (Global MTM Inc.) for their financial and technical support and cooperation over equipment setup and accessories development to enable the test program of this study. Special thanks are due to Farid Shabani for his technical support during different stages of development of the required accessories. The contributions of Dr. Ali Lashkari in his invaluable inputs in fundamental aspects of anisotropy are gratefully acknowledged.

9 REFERENCES

Ahmad A. and Fakharian K. 2020. Effect of stress rotation and intermediate stress ratio on monotonic behavior of granulated rubber–sand mixtures. *J. Mater. Civ. Eng. ASCE*, 32, 1–11. https://doi.org/10.1061/(ASCE)MT.1943-5533.0003054

ASTM D6913–04. 2009. Standard test methods for particle-size distribution (gradation) of soils using sieve analysis. (2009)

Cheng Z. and Wang J. 2018. Experimental investigation of inter-particle contact evolution of sheared granular materials using X-ray micro-tomography. *Soils & Foundations*, 58, 1492–1510. https://doi.org/10.1016/j.sandf.2018.08.008

Chern J. C. 1981. Effect of static shear on resistance to liquefaction. Doctoral dissertation*, University of British Columbia*.

Eghbali A.H. amd Fakharian K. 2014. Effect of principal stress rotation in cement-treated sands using triaxial and simple shear tests. *Int. J. Civ. Eng.* 12(1), 1–14.

Fakharian K., Eghbali A.H., Heidari Golafzani S., Khanmohamadi M. 2018. Specimen preparation methods for artificially cemented sand in simple shear and hollow cylinder apparatuses. *Scientica Iranica, Transaction A, Civil Engineering*, 25(1), 22–32. http://dx.doi.org/10.24200/sci.2017.4177

Fakharian K. and Kaviani-Hamedani F. 2020. Influence of Initial Anisotropy, Stress Path and Principal Stress Rotation on Monotonic Behavior of Clean and Mixed Sands, in: *Key Engineering Materials*. 587, pp. 417–430.

Fakharian K., Kaviani-Hamedani F., Parandian I., Aghdam M.J. 2019. Investigation of fabric evolution using bidirectional shear wave velocity measurements, in: E3S Web of Conferences, 7th Int. Symposium on Deformation Characteristics of Geomaterials (IS-Glasgow 2019), 92, p. 3008. http://doi.org/10.1051/e3sconf/20199203008

Fakharian K. and Vafaie N. 2021. Effect of density on skin friction response of piles embedded in sand by simple shear interface tests. *Canadian Geotechnical Journal*, 58(5), 619–636. https://doi.org/10.1139/cgj-2019-0243

Fakharian K., Kaviani-Hamedani F. and Imam S.M.R. 2021. Influences of Initial Anisotropy and Principal Stress Rotation on the Undrained Monotonic Behavior of a Loose Silica Sand. *Canadian Geotechnical Journal*. https://doi.org/10.1139/cgj-2020-0791

Gu X. Q. and Yang J. 2013. A discrete element analysis of elastic properties of granular materials. *Granul. Matter*, 15, 139–147.

Guo P. 2008. Modified Direct Shear Test for Anisotropic Strength of Sand. *J. Geotech. Geoenvironmental Eng. ASCE,* 134, 1311–1318.

Harilal R. and Ramji M. 2014. Adaptation of open source 2D DIC software Ncorr for solid mechanics applications. *9th Int. Symp. Adv. Sci. Technol. Exp. Mech*

Kaviani-Hamedani F. Fakharian K. & Lashkari A. 2021. Bidirectional Shear Wave Velocity Measurements to Track Fabric Anisotropy Evolution of a Crushed Silica Sand during Shearing. *Journal of Geotechnical and Geoenvironmental Engineering*, 147(10), 04021104. https://doi.org/10.1061/(ASCE)GT.1943-5606.0002622

Lashkari A. Karimi A. Fakharian K. Kaviani-Hamedani F. 2017. Prediction of undrained behavior of isotropically and anisotropically consolidated Firoozkuh sand: instability and flow liquefaction. *Int. J. Geomech, ASCE.* 17(10), 4017083.https://doi.1061/(ASCE)GM.1943-622.0000958

Li X. and Li X. S. 2009. Micro-macro quantification of the internal structure of granular materials. *Journal of engineering mechanics*. 135, 641–656.

Li X.S. and Dafalias Y.F. 2012. Anisotropic Critical State Theory: Role of Fabric. *J. Eng. Mech*. 138, 263–275.

Masson S. and Martinez J. 2001. Micromechanical analysis of the shear behavior of a granular material. *J. Eng. Mech*. 127, 1007–1016.

Miura S. Toki S. Nakakuki S. 1982. A sample preparation method and its effect on static and cyclic deformation-strength properties of sand. *Soils and foundations* 22, 61–77.

Nakakuki S. and Oda M. 1972. The mechanism of fabric changes during compressional deformation of sand. *Soils and foundations* 12, 1–18.

Roscoe K.H. Schofield A.N. Wroth C.P. 1958. On the yielding of soils. *Geotechnique* 8, 22–53. https://doi.org/10.1680/geot.1958.8.1.22

Schofield A. Wroth P. Shepley P. 1968. Critical state soil mechanics (Vol. 310). London: McGraw-hill.

Shirley D.J. and Hampton L.D. 1978. Shear-wave measurements in laboratory sediments. *J. Acoust. Soc. Am*. 63, 607–613.

Styler M.A. and Howie J.A. 2014. Continuous monitoring of bender element shear wave velocities during triaxial testing. *Geotech. Test. J.* 37, 218–229.

Tatsuoka F. Ochi K. Fujii S. Okamoto M. Nakakuki S. 1986. Cyclic undrained triaxial and torsional shear strength of sands for different sample preparation methods. *Soils and foundations* 26, 23–41.

Vafaei N. Fakharian K. and Sadrekarimi A. (2021). Sand-Sand and Sand-Steel Interface Grain-scale Behavior under Shearing. *Transportation Geotechnics*, 30, 100636.

Verdugo R. and Ishihara K. 1996. The steady state of sandy soils. *Soils and foundations*. 36, 81–91.

Wang Y.H. and Mok C.M. 2008. Mechanisms of small-strain shear-modulus anisotropy in soils. *J. Geotech. geoenvironmental Eng*. 134, 1516–1530.

Yan W.M. and Zhang L. 2013. Fabric and the critical state of idealized granular assemblages subject to biaxial shear. *Comput. Geotech*. 49, 43–52.

Yang L.-T.T. Li X. Yu H.-S.S. Wanatowski D. 2016. A laboratory study of anisotropic geomaterials incorporating recent micromechanical understanding. *Acta Geotech*. 11, 1111–1129. https://doi.org/10.1007/s11440-015-0423-7

Yu H. Zeng X. Li B. Ming, H. 2013. Effect of fabric anisotropy on liquefaction of sand. *J. Geotech. geoenvironmental Eng*. 139, 765–774.

Zhao J. Guo N. 2013. A new definition on critical state of granular media accounting for fabric anisotropy, in: *AIP Conference Proceedings. pp*. 229–232.

Zhao J. Guo N. Li X.S. 2013. Unique critical state characteristics in granular media considering fabric anisotropy. *Géotechnique* 63, 695.